SCIENTIFIC REPORTS
nature research

Check for updates

OPEN

5G planar branch line coupler design based on the analysis of dielectric constant, loss tangent and quality factor at high frequency

Nor Azimah Mohd Shukor & Norhudah Seman✉

This study focuses on the effect of different dielectric properties in the design of 3-dB planar branch line coupler (BLC) using RT5880, RO4350, TMM4 and RT6010, particularly at high frequency of 26 GHz, the fifth generation (5G) operating frequency. The analysis conducted in this study is based on the dielectric constant, loss tangent and quality factor (Q-factor) associated with the dielectric properties of the substrate materials. Accordingly, the substrate that displayed the best performance for high frequency application had the lowest dielectric constant, lowest loss tangent and highest Q-factor (i.e., RT5880), and it was chosen to enhance our proposed 3-dB BLC. This enhanced 3-dB BLC was designed with the inclusion of microstrip-slot stub impedance at each port for bandwidth enhancement, and the proposed prototype had dimensions of 29.9 mm × 19.9 mm. The design and analysis of the proposed 3-dB BLC were accomplished by employing CST Microwave Studio. The performance of scattering parameters and the phase difference of the proposed BLC were then assessed and verified through laboratory measurement.

Due to the rapid advancements in wireless communications, a sophisticated communication system that includes high-performance devices necessary to deploy next (i.e., fifth) generation (5G) technologies. This system requires devices that further perfect wireless communication between anything, anywhere and at any time[1]. The 5G were deployed in several countries including South Korea, the United Kingdom, Germany and the United States and many more countries are expected to deploy 5G soon and the high demand for 5G technology, which require 24/7 ubiquitously high-speed connectivity become a significant challenge for researchers and engineers involved in the development of radio frequency (RF) and microwave components, antenna design, and network planning. Butler matrix design is particularly high-demand in 5G application because the Butler matrix can be employed to support the control capability of beam-forming and electric scanning antennas[2].

The Butler matrix was first introduced by Jesse Butler and Ralph Lowe[3] and the beam-forming network creates multiple fixed overlapping beams to cover the designated angular area[4]. Since it is an N × N passive reciprocal network, it can be used to transmit and receive signals[5,6]. There are several properties associated with the Butler matrix, including inputs that are isolated from each other, phases of N outputs that are linear with respect to position and a phase increment between the outputs that depends on the selection of input[4]. The Butler matrix is also capable of beam-steering with uniform amplitude and adequate phase difference between consecutive output ports[5]. The power at the input port of the Butler matrix is equally distributed to the output ports[4] and the configuration of the Butler matrix essentially consists of passive components such as a branch line coupler (BLC), a phase shifter and crossover[7,8]. A non-conventional configuration BM has been proposed by Babale et al.[9], where the BM was constructed without using crossover and phase shifter, however it was not practical for cascaded BM due to the position of input and output ports, which may lead to the connection issues. As the most critical component in the Butler matrix configuration, the BLC designed during the first stage must display good performance. Since a BLC is only capable offering narrowband performance, many studies related to bandwidth improvement have been performed. The defect ground structure (DGS) technique can be employed under the branch arm of the BLC for to improve bandwidth[10]. Employing the DGS technique able to enhance the bandwidth of the BLC design[10] by 8.2% compared to conventional BLCs.

Wireless Communication Centre (WCC), School of Electrical Engineering, Universiti Teknologi Malaysia (UTM), 81310 UTM Johor Bahru, Johor, Malaysia. ✉email: huda@fke.utm.my

Then, a dumbbell-shaped DGS was etched on the ground plane of another BLC[11] design. In the design, a 120Ω transmission line was used to replace the quarter-wavelength 150Ω transmission line. The performance of this design indicated that the good results could be achieved within a frequency range of 1.85–3.35 GHz with a bandwidth enhancement of approximately 20%. However, the disadvantage of using a DGS is that it is only suitable to be implemented with the high line impedance. Another technique that use a slotted line on a BLC was introduced to further improved bandwidth[12]. The slotted line was placed at the ground plane and positioned beneath the vertical branches of the BLC design. It was concluded that slot dimensions (i.e., $W \times L$) of 0.7 mm × 11.5 mm resulted in the best BLC performance within a frequency range of 3.5–4.7 GHz[12]. This BLC design[12] has improved bandwidth by 80% compared to conventional BLCs. Another 3-dB BLC with improved bandwidth proposed by Jin and Xu[13] by introducing the artificial magnetic conductor (AMC). The design comprised of a spacer with hollow interspace in the middle layer that sandwiched by AMC patches at the upper layer and microstrip coupler which printed on the upper surface of the bottom substrate layer. This multilayered coupler structure faced misalignment between each layer and air gap in the fabrication stage that led to a significant impact on the performance for high frequency applications. Thus, the implementation of a single substrate in the coupler design at high frequency is preferable.

Another crucial aspect in designing the coupler is the planar dielectric material, which is also known as the substrate. The parameters of the substrate are not only focused on the degree of design miniaturization but also influences the quality factor (Q-factor) of the components. The effect of different dielectric constants, ε_r towards coupler size has been presented by Letavin Denis et al.[14] concerning Rogers RT ($\varepsilon_r = 3$) and FR-4 ($\varepsilon_r = 4.4$), and design frequency of 2 GHz. The authors stated that FR-4 substrate has a better effect on the miniaturization of coupler compared to Roger RT due to its higher dielectric constant. However, miniaturization is not a concern in the design at high frequency. The components[7,14,15] designed on FR-4 substrate due to its low cost, with FR-4 having a high loss tangent. Since FR-4 displays a high loss tangent, it may degrade the Q-factor of the design, which leads to the degradation of performance compared to the performance of the designs with RO4003C[6] and RT5870[16]. Authors have added that the measured performance is also degraded due to several other factors, such as conduction losses and dielectric losses[7, 17]. Hence, FR-4 is not suitable for high-frequency design due to its high dissipation factor, which results in higher losses as the frequency increases[18]. Therefore, the FR-4 substrate is not considered suitable for high operating frequency design. Thus, most of the researchers are having a tendency to select the high-performance substrate material over FR-4 substrate for high frequency design due to this impact of high loss tangent, which will significantly affect the performance of the circuit. The dielectric losses of the substrates are closely related to the dissipation factor and the loss tangent, which are proportional to the frequency[17]. Despite, loss tangent seems to be a clear factor in the substrate selection, other dielectric properties' effects toward the design such as dielectric constant and Q-factor are required to be carefully studied at high frequency together with loss tangent to ensure a good performance can be accomplished particularly for microstrip implementation. The effects due to dielectric constant and Q-factor cannot be known from the manufacturer datasheet without systematic study and analysis.

The remainder of this paper is organized in the following manner. Next section introduces the analysis of different substrates having different properties with respect to the dielectric constant, loss tangent, and Q-factor associated with dielectric properties and their relationship to BLC performance was observed. The enhanced BLC design was then proposed with the implementation of microstrip-slot stub impedance at each port's transmission line. The performance was simulated and measured. It was then compared to the conventional design and other designs using different techniques, and discussed thoroughly.

Methods

Selecting the best substrate to be incorporated into the design is crucial, especially at higher operating frequencies used in 5G wireless communication applications. Therefore, in this study, the analysis of a single-section planar BLC with different substrates was conducted. Questions arise regarding which substrate among the available high-performance substrates offers the best performance for the 3-dB BLC design at the designated frequency. The analysis in this study is based on the dielectric constant, loss tangent, Q-factor and their relationship to BLC performance.

Analysis of different substrates. The characteristics of different substrates can affect the overall performance of the design. Four different substrates were selected for analysis, including RT5800, RO4350, TMM4 and RT6010, which were chosen due to their excellent performance at higher frequencies. Each of the four substrates has a different dielectric constant and loss tangent, while the thickness of the substrate was fixed at 0.254 mm. The properties of each substrate are summarized in Table 1.

RT5880, which is made of glass microfiber reinforced polytetrafluoroethylene (PTFE) composite, displayed the lowest dielectric constant (2.2) among all the chosen high laminating frequency substrates, the lowest loss tangent (0.0009), and a negative thermal coefficient of − 125 ppm/°C[19]. Since RT5880 has a low dielectric constant, it is suitable for high frequency applications because the electrical losses and dispersion is considered to be minimal[19]. Meanwhile, the RO4350 substrate, which is a woven glass reinforced hydrocarbon ceramic laminate displayed second-lowest dielectric constant (3.66), the highest loss tangent (0.0037), and the highest positive thermal coefficient of + 50 ppm/°C[20]. This substrate provided tight control of the dielectric constant and displayed low loss[19]. The third substrate was TMM4, which is composed of a ceramic thermoset polymer composite with a dielectric constant (4.7), the second-lowest loss tangent (0.0020), and a low thermal coefficient of + 15 ppm/°C[21]. The electrical and mechanical properties of TMM4 laminates combine many of the benefits of both ceramic and traditional (PTFE) microwave circuit laminates[21]. Finally, the RT6010 substrate had the highest dielectric

Substrate	Material	Dielectric Constant, ε_r	Loss Tangent, tan δ	Thickness *h* (mm)	Thermal Coefficient (ppm/°C)	Condition (GHz)
RT5880	Glass microfiber reinforced PTFE composite	2.2	0.0009	0.254	−125	8–40
R04350	Woven glass reinforced hydrocarbon ceramic	3.66	0.0037	0.254	+50	8–40
TMM4	Ceramic thermoset polymer composite	4.7	0.0020	0.254	+15	8–40
RT6010	Ceramic PTFE composite	10.7	0.0023	0.254	−425	8–40

Table 1. The substrates with the different materials and dielectric properties.

constant (10.7) with negative thermal coefficient of −425 ppm/°C[18]. Furthermore, this substrate also displayed low loss with loss tangent of 0.0023[22].

Generally, when selecting a dielectric material during the design process, two parameters are considered, including the dielectric constant and loss tangent. The loss tangent, tan δ defines the measure of signal loss as the signal propagates through the transmission line, and can be expressed as (1)[23,24]:

$$\tan\delta = \frac{\omega\varepsilon_r'' + \sigma}{\omega\varepsilon_r'} \tag{1}$$

where ε_r' and ε_r'' are the real and imaginary part of the complex relative permittivity, ε_r^*, respectively. Meanwhile, ω and σ are angular frequency and conductivity, respectively with conditions of $\varepsilon_r'' \geq 0$ and $\varepsilon_r' \gg \varepsilon_r''$. The real part of ε_r^*, which is ε_r' associated to the ability of a material to store the incident electromagnetic (EM) energy through wave propagation, while, the imaginary part of ε_r^* is denoted by ε_r'' related to the degree of EM energy losses in the material. Thus, ε_r' and ε_r'' are also known as the dielectric constant, ε_r and the loss factor, respectively. At high frequencies that were considered in this proposed work, the substrate's loss tangent, tan δ can be simplified to $\varepsilon_r''/\varepsilon_r'$. It is also known as the dissipation factor that describes the angle difference between capacitance current and voltage. Hence, a lower loss tangent is required in the substrate to ensure low dielectric loss and low dielectric absorption[25]. These two parameters, ε_r and tan δ are directly related to the Q-factor due to the dielectric, Q_d that can be expressed as (2)[26]:

$$Q_d = 27.3\frac{\sqrt{\varepsilon_{eff}}}{\alpha_d \lambda_0} \tag{2}$$

where the ε_{eff}, λ_0 and α_d are the effective dielectric constant, the wavelength in the air and dielectric loss, respectively. The ε_{eff} can be defined by (3)[23]:

$$\varepsilon_{eff} = \frac{\varepsilon_r + 1}{2} + \frac{\varepsilon_r - 2}{2}\frac{1}{\sqrt{1 + 12h/W_m}} \tag{3}$$

where h and W_m are the thickness of the substrate and the width of the microstrip transmission line, respectively, while, the dielectric loss, α_d can be expressed as (4)[26]:

$$\alpha_d = 27.3\frac{\varepsilon_r\left(\varepsilon_{eff} - 1\right)\tan\delta}{\sqrt{\varepsilon_{eff}}\left(\varepsilon_r - 1\right)\lambda_o} \tag{4}$$

Thereafter, an analysis of the Q-factor associated with the material's dielectric properties, Q_d was performed through calculation implementing (2)–(4) to observe the effect of different substrates, including RT5880, RO4350, TMM4 and RT6010, which have a different dielectric constant, ε_r and loss tangent, tan δ. The width of the microstrip transmission line, W_m that correspond to 50Ω was used in this analysis. The relationship between Q_d and the different ε_r of RT5880, RO4350, TMM4 and RT6010 substrates, and the relationship between Q_d and tan δ are depicted in Figs. 1 and 2.

As presented in Fig. 1, RT5880, RO4350, TMM4 and RT6010 substrates have Q_d values of 1302.79, 302.56, 549.70 and 458.69, respectively. It is important to note that Q_d generally decreases as the value of ε_r increases as depicted by the proportional correlation between Q_d and ε_{eff} , which is calculated using Eq. (2), where RT5880 has the highest Q_d and the lowest ε_r. However, this trend does not apply to RO4350 that had the second-lowest ε_r and the lowest performance of Q_d. Hence, by referring back to Eqs. (2) and (4), setting aside the dielectric constant, ε_r, Q_d is inversely proportional to dielectric loss, α_d. Consequently, this α_d is determined by ε_r and tan δ as expressed in Eq. (4). Since α_d is proportional to tan δ, and Q_d is inversely proportional to α_d, thus Q_d is inversely proportional to tan δ. Meanwhile since α_d is a function of ε_r, the influence of tan δ towards Q_d is greater compared to ε_r, which can be observed from the plot in Fig. 2. Referring to Fig. 2, the value of Q_d decreases as the value of tan δ increases. Therefore, even though RO4350 has the second-lowest ε_r, it has the highest tan δ among the substrates, which led to the lowest Q_d performance.

Generally, this behavior can be explained by the characteristics of the ε_r that is influenced by ionic or electronic polarization, which generates α_d in the presence of electromagnetic wave[27]. The increasing value of ε_r provides a higher α_d value as the electric field intensity inside the dielectric layer increases[23]. RT5880 and RT6010 have polytetrafluoroethylene (PTFE) in their composition, while TMM4 has a polymer with low thermal

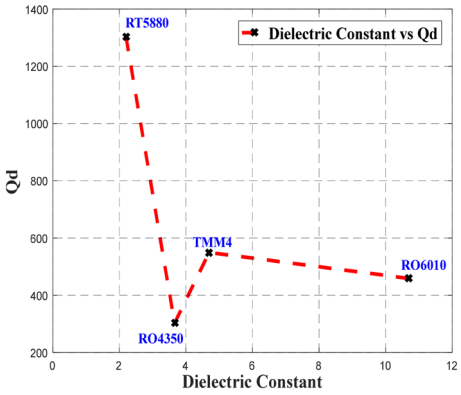

Figure 1. The relation between the Q-factor associated with the dielectric properties, Q_d and dielectric constant of the different substrates.

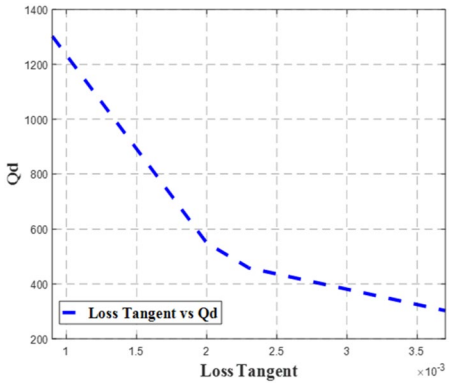

Figure 2. The relation between the Q-factor associated with the dielectric properties, Q_d and loss tangent, tan δ.

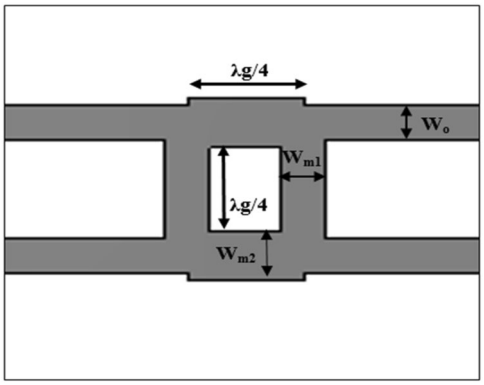

Figure 3. The design of the single-section 3-dB branch line coupler.

conductivity, an excellent coefficient of thermal expansion (CTE), and low processing temperature, which results in low α_d [28] as presented in Table 1. While, glass is a good thermal and homogeneity insulator, it also displays a high dielectric loss[28]. To obtain a lower α_d value and maintain the advantages of glass, glass-reinforced ceramics can be used as displayed by R04350[28]. In any event, the dielectric loss of R04350 is still higher than RT5880, TMM4 and RT6010. Following this analysis of the four substrates, further analysis was performed by employing a single-section planar 3-dB BLC design.

Analysis of BLC using different substrates. Figure 3 presents the design of the single-section 3-dB BLC. The common microstrip equation is denoted as (5), which was used to compute W_o, W_{m1} and W_{m2}, where W_o and W_{m2} refer to the characteristics of 50Ω, while W_{m1} refer to those of 35Ω[23]:

Parameters	Substrates/dimensions (mm)			
	RT5880	RO4350	TMM4	RT6010
W_{m1}	0.8	0.65	0.5	0.25
W_{m2}	1.1	0.9	0.6	0.5
W_o	0.8	0.65	0.5	0.25
$\lambda_g/4$	2.12	1.71	1.54	1.08

Table 2. Dimensions of single-section 3-dB BLCs using different substrates.

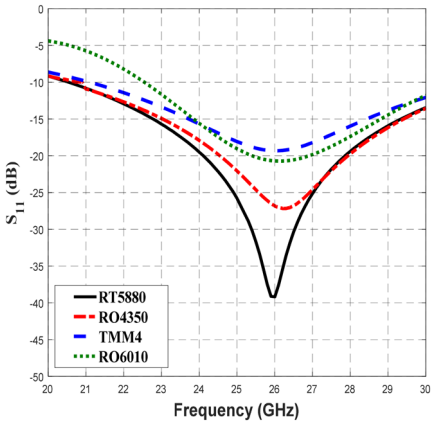

Figure 4. The reflection coefficients, S_{11} of the 3-dB BLC with different substrates.

$$\frac{W_m}{h} = \frac{2}{\pi}\left[B - 1 - \ln(2B-1) + \frac{\varepsilon_r}{2\varepsilon_r}\left\{\ln(B-1) + 0.39 - \frac{0.61}{\varepsilon_r}\right\}\right] \tag{5}$$

where constant B can be expressed as (6)[23]:

$$B = \frac{377\pi}{2Z_0\sqrt{\varepsilon_r}} \tag{6}$$

where Z_0 is the characteristic impedance.

The guide wavelength, λ_g was then determined by (7)[29]:

$$\lambda_g = \frac{c}{f\sqrt{\varepsilon_{eff}}} \tag{7}$$

where c and f are the speed of light and design frequency, respectively. The properties for each substrate were used to design the 3-dB BLC, and the dimensions of the designed couplers were computed and optimized, which are summarized in Table 2. The performance of each BLC was then assessed based on S-parameters, phase difference and bandwidth.

The performance of each BLC was then assessed based on S-parameters, phase difference and bandwidth via simulation through the use of Computer Simulation Technology (CST) Microwave Studio software. Transient Solver tool was utilized with frequency range setting between 20 to 30 GHz and open boundary condition to calculate the energy transmission between various ports of the design structure. Figure 4 illustrates the reflection coefficient performance, S_{11} of the designed BLC with different substrates, which revealed that the S_{11} of the BLC designed with the RT5880 substrate was less than − 10 dB within a frequency range of 20.54–30 GHz. Meanwhile, the BLC design that employed the RO4350 substrate showed the performance of S_{11} was below − 10 dB across 21–30 GHz. In addition, the use of TMM4 and RT6010 offered S_{11} values that were less than − 10 dB in the ranges of 21.1–30 GHz and 22.55–30 GHz, respectively. Hence, the best S_{11} performance with the relatively broadest bandwidth and lowest S_{11} at 26 GHz, which is shown by the design that employed RT5880, which has the lowest ε_r and lowest tan δ among all four substrates was expected to have the lowest loss.

Figure 5 shows the transmission coefficient of S_{21} when different substrates were used in the design of the BLC. Similar S_{21} performance of − 3 dB with ± 1 dB deviation were obtained for RT5880, RO4350, TMM4, and RT6010 for slightly different frequency ranges of 21.14–30 GHz, 21.9–30 GHz, 23.18–30 GHz and 24.28–30 GHz, respectively. Compared to S_{11} performance, BLC design with RT5880 displayed the widest frequency range of 8.86 GHz with S_{21} performance of − 3 dB ± 1 dB. Meanwhile Fig. 6 depicts the coupling output, S_{31} that specifies the ratio of input power, P_1 to the coupled power, P_3 for BLC design that utilized different substrates. The

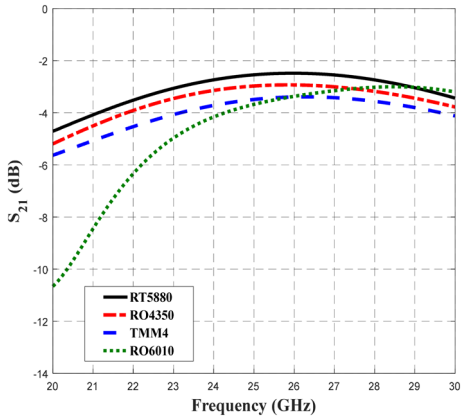

Figure 5. The transmission coefficients, S_{21} of the 3-dB BLC design using different substrates.

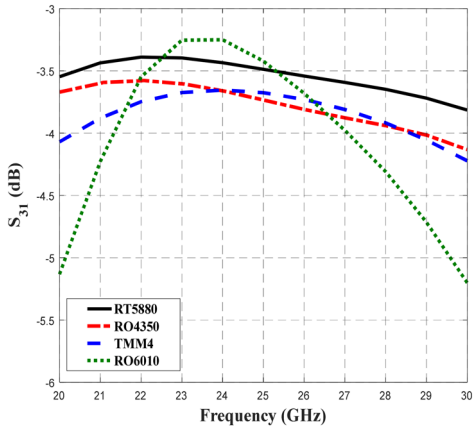

Figure 6. The coupling performance, S_{31} of the BLC design by using different substrates.

results of our analysis indicated that the performance of S_{31} was −3 dB ± 0.9 dB within a frequency range of 20–30 GHz when RT5880 substrate was used in the design, while, the coupling performance was −3 dB ± 1 dB when the RO4350 substrate was used in a range of 20–28.74 GHz. Furthermore, similar performances of S_{31} were achieved when the design utilized TMM4 and RT6010 substrates, which were − 3 dB ± 1 dB in a frequency range of 20.34–28.62 GHz and 21.28–27.07 GHz, respectively. Hence, a coupling coefficient of 3-dB with the lowest deviation across the widest frequency range was achieved by the BLC design utilized onto RT5880 substrate. The next important analysis is associated with S_{41} performance, which involves the responses obtained from the BLC design with different substrates as depicted in Fig. 7. In this design, the lowest isolation performance was set to be 10 dB. As shown in Fig. 7, the performance of S_{41} was less than − 10 dB within a frequency range of 20–30 GHz for the design that employed all substrates. In this analysis, the lowest S_{41} performance at 26 GHz shown by the design that employed RT5880.

Therefore, the analysis proceeded to consider the phase difference between output ports. In this design, the deviation of the phase difference between the output ports was set to ± 2° from the ideal of 90°. Based on the phase difference analysis shown in Fig. 8, a BLC phase difference of 90° ± 2° are demonstrated by designs that employed RT5880, RO4350, TMM4 and RT6010 substrates across slightly different frequency ranges of 24.52–30 GHz, 25.52–29.17 GHz, 25.5–28 GHz and 24.81–27.73 GHz, accordingly. Similarly, as in the analysis of S_{11}, S_{21}, S_{31} and S_{41}, the design with RT5880 displayed the best phase performance across the widest frequency range, which is likely because it has the lowest ε_r and lowest tan δ. The performances of S_{11}, S_{21}, S_{31}, S_{41} and the phase difference between output ports are summarized in Table 3. The Q-factor associated with the material's dielectric properties, Q_d that was obtained through the analysis of those dielectric properties is presented in Table 3 for further comparison and analysis.

Table 3 shows that the widest bandwidth performance of 5.48 GHz (21.1%) was achieved when the RT5880 substrate was used in the BLC design. Referring to Table I, RT5880 has the lowest ε_r of 2.2 and lowest tan δ of 0.0009 which resulted in the highest Q_d of 1302.79. Meanwhile, RT6010 displayed the narrowest bandwidth performance of 2.26 GHz (8.7%) and it has the highest ε_r of 10.7 and second-highest tan δ of 0.0023, which lead to a lower Q_d of 458.69. The RO4350 substrate with the highest tan δ of 0.0037 and the second-lowest ε_r of 3.6 and displayed the lowest Q_d of 302.56, though it also had the second-widest bandwidth performance of 3.22 GHz

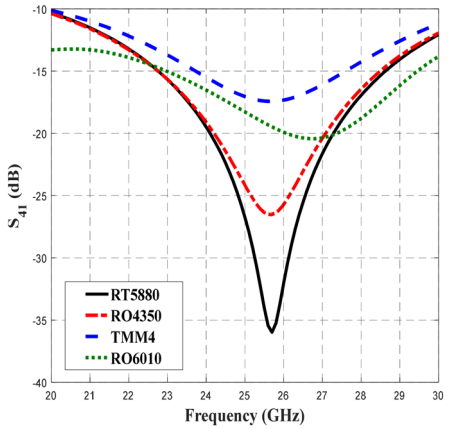

Figure 7. The S_{41} performance of the 3-dB BLC design with different substrates.

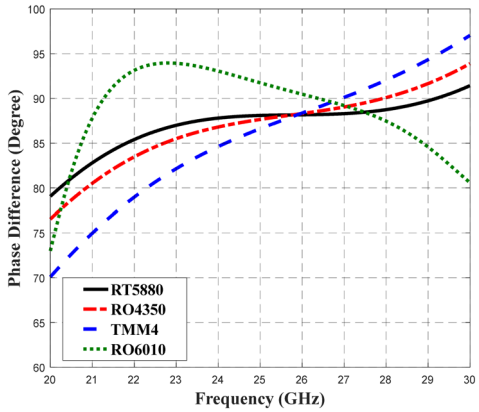

Figure 8. The phase difference performance of the 3-dB BLC design with the use of different substrates.

Parameters	Substrates/dimensions (mm)			
	RT5880	RO4350	TMM4	RT6010
S_{11} (dB)	< − 10	< − 10	< − 10	< − 10
S_{21} (dB)	− 3 ± 1	− 3 ± 1	− 3 ± 1	− 3 ± 1
S_{31} (dB)	− 3 ± 0.9	− 3 ± 1	− 3 ± 1	− 3 ± 1
S_{41} (dB)	< − 10	< − 10	< − 10	< − 10
Phase Difference (Degree)	90 ± 2	90 ± 2	90 ± 2	90 ± 2
Operating Frequency (GHz)	24.52–30	25.52–28.74	25.5–28	24.81–27.07
Bandwidth, GHz (%)	5.48 (21.1)	3.22 (12.4)	2.5 (9.6)	2.26 (8.7)
Q_d	1302.79	302.56	549.70	458.69

Table 3. The performance of 3-dB BLC design with different substrates and the respective Q_d.

(12.4%). Even though a lower tan δ significantly contributes to a higher Q_d compared to ε_r, results indicated that the ε_r is a primary factor in the determination of optimal bandwidth performance with an inversely proportional relationship. The ε_r of a material represents the ability of that material to store electrical energy in the presence of an electrical field, whereas, when the frequency increases, the losses in the substrate begins to reduce the ability of the dielectric material to store energy. Therefore, it can be concluded that the bandwidth performance increases as the dielectric constant decreases, while the high dielectric constant substrate may lose its ability of storing energy. Thus, based on the results of our analysis, the substrate with a low dielectric constant and a low tan δ, which contribute to the respective high bandwidth and high Q-factor is the most suitable for 5G applications at high frequencies, and in this case, a design frequency of 26 GHz that uses the RT5880 substrate was selected.

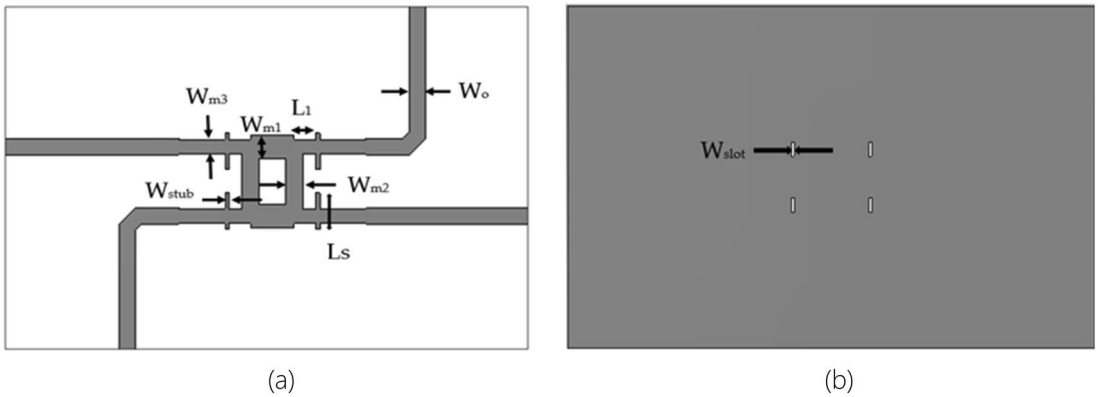

Figure 9. The proposed 3-dB BLC with the implementation of microstrip-slot stub at each port; (**a**) top view and (**b**) bottom view.

Design of 3-dB BLC with microstrip-slot stub. This section discusses the proposed wideband 3-dB BLC design, as depicted in Fig. 9, with the implementation of a microstrip-slot stub for bandwidth improvement over that of conventional BLC designs, as shown in Fig. 3 by using CST Microwave Studio with the utilization of Transient Solver tool, frequency range setting between 20 to 30 GHz and open boundary condition. The best substrate was RT5880 based on the analysis of its dielectric properties, and was thus chosen for the design. The proposed microstrip-slot stub impedance was placed at each port at a distance, L_1 from the BLC. By tuning these microstrip-slot stub impedances, better matching can be achieved to ensure maximum power is transferred from the source, and a minimum signal is reflected from the load, which consequently enhances the bandwidth[30,34].

Generally, the input impedance of the stub, Y_{in} can be written as (8)[31]:

$$Y_{in} = jY_0 \tan\theta_{stub} \tag{8}$$

where Y_0 and θ_{stub} are the stub admittance and the electrical length of the stub, respectively, and the θ_{stub} can be expressed as (9)[31]:

$$\theta_{stub} = \beta L_s = \frac{\omega_0}{V_{pstub}} L_s \tag{9}$$

where ω_0, L_s and V_{pstub} are the angular frequency, the length of stub and the phase velocity of the stub, respectively. By comparing $Y = \omega C$ to Eq. (8), the length of the stub, L_s can be obtained in (10)[31]:

$$\omega_0 C = \frac{1}{Z_{stub}} \tan\left(\frac{\omega_0}{V_{pstub}}\right) L_s \tag{10}$$

where Z_{stub} is the characteristic impedance of the stub. It was stated that junction discontinuities can be avoided when the length of stub impedance is half the wavelength[28]. However, the parameters still need to be optimized to achieve optimal performance. To achieve optimal performance, a stub with a higher impedance is required[32].

Furthermore, stub impedance can form reflection zeroes at equal distances on both sides of the ports[30]. The distance of the stub impedance of the proposed BLC design is defined as L_1. Referring back to the common matching technique that employs the stub[23], the load impedance, Z_L representing the BLC can be expressed as (11):

$$Z_L = \frac{1}{Y_L} = R_L + jX_L \tag{11}$$

where Y_L, R_L and X_L are the load admittance, the real part of load impedance and the imaginary part of load impedance, respectively. Therefore, the impedance at a distance, L_1 from the load (BLC) is given in the (12) and (13):

$$Z_{L1} = Z_0 \frac{(R_L + jX_L) + jZ_0 t}{Z_0 + j(R_L + jX_L)t} \tag{12}$$

and

$$t = \tan\beta L_1 \tag{13}$$

Let the admittance of stub impedance at a distance, L_1 be expressed as (14):

$$Y_{L1} = G + jB = \frac{1}{Z_{L1}} \tag{14}$$

where parameters G and B can be defined by (15) and (16), respectively, by using (13) and (14):

Parameters	Dimension (mm)
W_{m1}	1.09
W_{m2}	0.8
W_{m3}	0.7
W_{slot}	0.15
L_1	0.65
L_s	0.85
W_o	0.8
λg/4	2.12

Table 4. Dimensions of proposed 3-dB Branch Line Coupler.

$$G = \frac{R_L\left(1 + \tan^2 \beta L_1\right)}{R_L^2 (X_L + Z_0 \tan \beta L_1)^2} \tag{15}$$

and

$$B = \frac{R_L^2 \tan \beta L_1 - (Z_0 - X_L \tan \beta L_1)(X_L + Z_0 \tan \beta L_1)}{Z_0\left[R_L^2 (X_L + Z_0 \tan \beta d)^2\right]} \tag{16}$$

Then, by equating $G = Y_0 = 1/Z_0$ and from (13)[23],

$$\frac{1}{Z_0} = \frac{R_L\left(1 + t^2\right)}{R_L^2 + (X_L+)} \tag{17}$$

Therefore, the value of t can be expressed as (18):

$$t = \begin{cases} \frac{X_L \pm \sqrt{\frac{R_L\left[(Z_0 - R_L)^2 + X_L^2\right]}{Z_0}}}{R_L - Z_0}, & for \quad R_L \neq Z_0 \\ \frac{-X_L}{2Z_0}, & for \quad R_L = Z_0 \end{cases} \tag{18}$$

Thereafter, by assuming $R_L = Z_0$ and by using $t = \tan \beta L_1 = \tan \frac{2\pi}{\lambda} L_1$, the distance of stub impedance from BLC, L_1 can be determined using (19):

$$\frac{L_1}{\lambda} = \begin{cases} \frac{1}{2\pi} \tan^{-1} t, & for \quad t \geq 0 \\ \frac{1}{2\pi}\left(\pi + \tan^{-1} t\right), & for \quad t > 0 \end{cases} \tag{19}$$

A narrow slot line is then employed at the ground plane underneath the microstrip stub to form microstrip-slot stub impedance because the use of the slot line can improve the bandwidth performance due to its slow-wave characteristic. The implementation of slot-line on the ground plane disturbs current distribution and this disturbance changes the characteristics of the transmission line, such as capacitance and inductance, to produce the slow-wave characteristics, which can increase the phase velocity delay. The characteristic impedance of the microstrip-slot stub can be determined through the use of the microstrip-slot line impedance, Z_{m-s} equation as expressed in (20)[33]:

$$Z_{m-s} = 18.22(W_{slot})^2 + Z_m \tag{20}$$

Obtaining the initial dimensions through calculation, this proposed BLC was simulated and optimized accordingly. The optimized dimensions of the coupler, as depicted in Fig. 9 were $W_o = 0.8$ mm, $W_{m1} = 1.09$ mm, $W_{m2} = 0.8$ mm, $W_{m3} = 0.7$ mm, $W_{stub} = 0.18$ mm, $W_{slot} = 0.15$ mm, $L_1 = 0.65$ mm, $L_s = 0.85$ mm and length of each branch, $\lambda/4 = 2.12$ mm. The dimensions of the proposed BLC are summarized in Table 4. The next objective is to verify the performance of the proposed BLC. Then, the proposed design was realized by employing the Roger RO5880 substrate with dielectric constant, ε_r of 2.2, a substrate thickness, h of 0.254 mm, and an overall size of 29.9 mm × 19.9 mm. Figure 10 shows the fabricated prototype of the proposed BLC with slotted-stub impedance.

Measurement of 3-dB BLC with microstrip-slot stub. The measurement of the proposed 3-dB BLC with microstrip-slot stub fabricated prototype was conducted using a vector network analyzer (VNA) to verify its performance. Prior to the measurement, the two-port network calibration procedure of VNA is necessary to remove its errors. The calibration was performed using the calibration standards involving the open, short, match, and through[35]. Following the completed calibration procedure, the measurement of the proposed BLC prototype was carried out with the setup as depicted in Fig. 11. Referring to the measurement setup, the selected ports were connected directly to the VNA, while the unused ports were terminated with 50 Ω SMA termination. Thereafter, a comparison was made in terms of the simulated and measured S-parameters and phase characteristics.

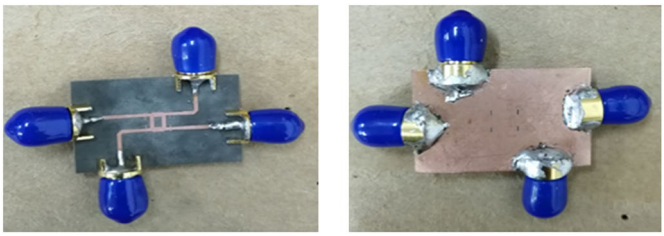

(a) (b)

Figure 10. The photography of the proposed 3-dB BLC prototype with the implementation of microstrip-slot stub impedance; (**a**) front view and (**b**) back view.

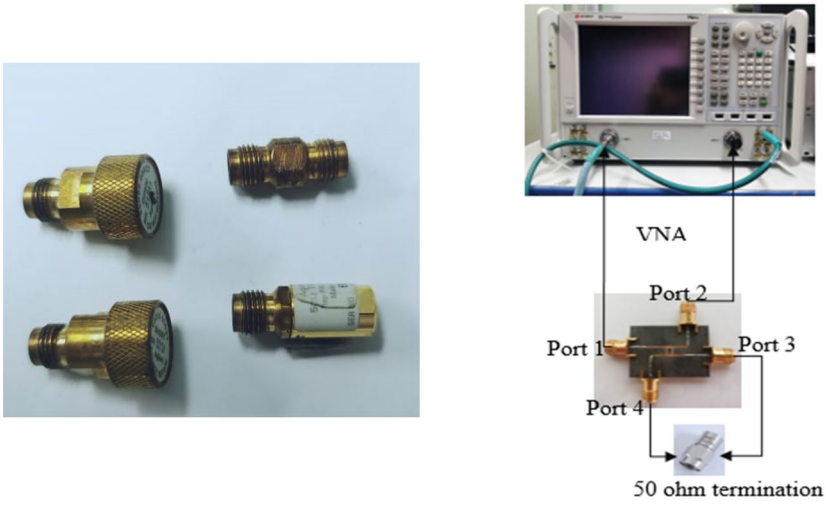

(a) (b)

Figure 11. (**a**) Calibration standards[36], and (**b**) the measurement setup of the proposed BLC using a vector network analyzer (VNA).

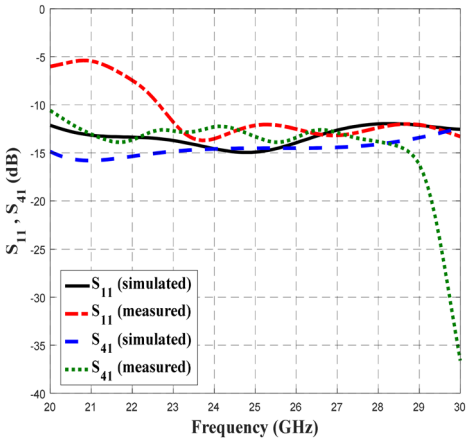

Figure 12. The simulated and measured S_{11} and S_{41} of the proposed BLC.

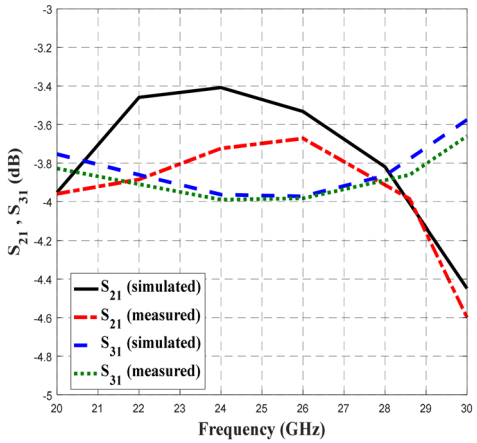

Figure 13. The simulated and measured S_{21} and S_{31} of the proposed BLC.

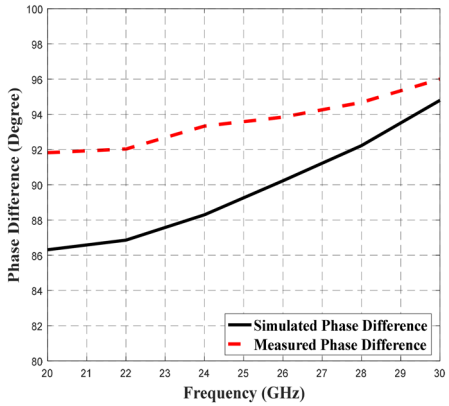

Figure 14. The simulated and measured phase difference of the proposed BLC.

Parameters	Initial BLC (RT5880)	Proposed BLC	
		Simulated	Measured
S_{11} (dB)	< − 10	< − 12	< − 11
S_{21} (dB)	− 3 ± 1	− 3 ± 1	− 3 ± 1
S_{31} (dB)	− 3 ± 0.9	− 3 ± 0.8	− 3 ± 0.9
S_{41} (dB)	< − 10	< − 12	< − 11
Phase Difference	90° ± 2°	90° ± 3°	90° ± 4°
Operating Frequency (GHz)	24.52–30	20–28.7	22–30
Bandwidth (GHz)	5.48 (21.1%)	8.7 (34.8%)	8 (32%)

Table 5. The simulated and measured performance of the proposed 3-dB BLC design.

Results and discussion

Figures 12,13 and 14 depict the simulated and measured performance of the proposed BLC, which operated well from 20 to 28.7 GHz and 22 to 30 GHz, respectively. As shown in Fig. 12, the simulated and measured S_{11} and S_{41} values were less than − 12 dB and − 11 dB, respectively. The value of − 10 dB and below used as the specification to indicate a good transmission signal from the input port to the output port, where almost 90% of the signal is being transmitted. Meanwhile based on the results presented in Fig. 13, the simulated and measured transmission coefficients at the coupling port (S_{31}) displayed a ± 1 dB deviation from the ideal value of 3 dB, while, the simulated and measured transmission coefficients of S_{21} depict the performance of − 3 dB ± 0.8 dB and − 3 dB ± 0.9 dB, respectively. Meanwhile, the plotted responses in Fig. 14 indicate that the simulated and measured phase differences between output ports were 90° ± 3° and 90° ± 4°, respectively. These S-parameters and phase difference performance are summarized in Table 5 to provide a clear comparison.

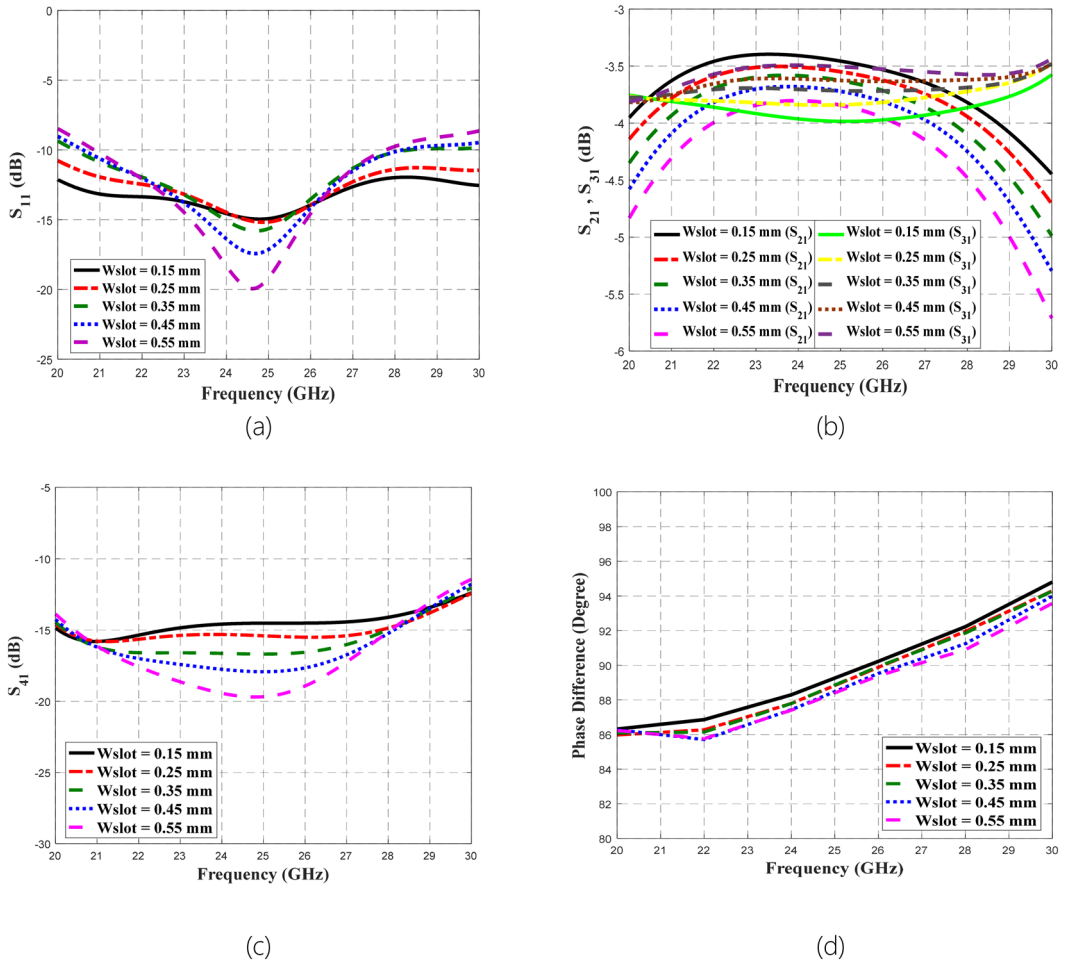

Figure 15. Parametric analysis on varied W_{slot} concerning (**a**) S_{11}, (**b**) S_{21} and S_{31}, (**c**) S_{41}, and (**d**) phase difference between output ports.

Based on the data in Table 5, the proposed BLC with microstrip-slot stub impedance at the ports' transmission line appeared to result in better performance of S_{11}, and S_{41} at a bandwidth was improved by approximately 2.52 GHz compared to initial single-section BLC design. Comparable transmission coefficients of S_{21} and S_{31} were observed between the proposed BLC and initial BLC designs. However, the phase difference between the output ports of the proposed BLC has deviated slightly more (± 1°) than initial BLC designs, but it was still within a reasonable performance range with respect to phase difference. Furthermore, performance of the simulated and measured BLC with microstrip-slot stub impedance were consistent with one another, along with an operating frequency that was slightly shifted. One of the main reasons that have been found affecting the measurement results was a small discrepancy in the width of the microstrip-slot stub impedance. To prove this, simulation on different widths of the microstrip-slot stub impedance was performed, analyzed, and discussed in the next sub-section.

Parametric analysis on different widths of the microstrip-slot stub impedance. Parametric analysis on different widths of the microstrip-slot stub impedance concerning its microstrip stub width, W_{stub} and slot line width, W_{slot} was performed via the use of CST Microwave Studio with a similar setting as in analysis and design in the section of Methods. Initially, the parametric analysis was started by fixing W_{stub} to its optimal dimension of 0.18 mm and varying W_{slot} between 0.15 mm and 0.55 mm. The effect of this varied W_{slot} was observed through S-parameters and phase difference as depicted in the following Fig. 15.

The function of slot implementation is to broaden the bandwidth due to its slow-wave characteristics. Concerning the bandwidth performance, it shows that from the plotted graphs in Fig. 15, the broadest bandwidth was provided by the smallest value of W_{slot} (0.15 mm) compared to the largest value of W_{slot} (0.55 mm). Besides, the smallest amplitude imbalance and phase imbalance were offered by 0.15 mm W_{slot}. Thus, the optimal W_{slot} dimension is 0.15 mm for this proposed coupler design. Any discrepancy from this optimal width will lead to deviation in the results of S-parameters and phase difference, in which the deviation trends can be observed through the plotted graphs. By comparing the plotted varied W_{slot} graphs to the summarized measured results in Table 5 and the assumption of fixed W_{stub} at 0.18 mm, it can be estimated that the fabricated coupler could have 0.35 mm W_{slot} instead of 0.15 mm. Afterward, the next concern is the effect of the varied W_{stub} towards the

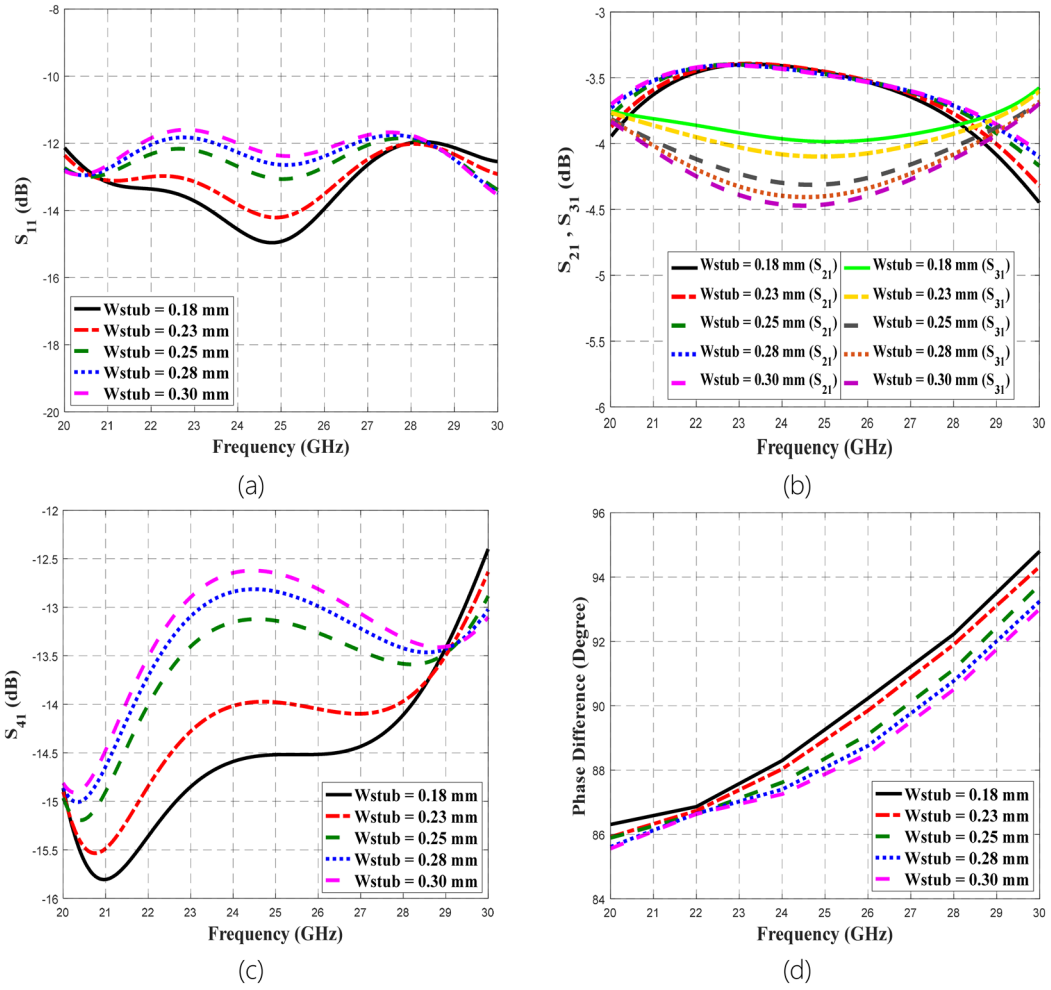

Figure 16. The parametric analysis on varied W_{stub} concerning (**a**) S_{11}, (**b**) S_{21} and S_{31}, (**c**) S_{41}, and (**d**) phase difference between output ports.

performance of the proposed BLC by fixing W_{slot} to its optimal dimension of 0.15 mm. W_{stub} was varied from 0.18 mm to 0.30 mm in this parametric analysis, which the effects on S-parameters and phase difference are shown in Fig. 16.

The addition of stub impedance in the design is to improve the matching, which consequently enhances the bandwidth performance compared to the design without stub impedance. Hence, W_{stub} increment from 0.18 mm to 0.30 mm can be seen affecting the matching and isolation of the coupler, which noted through the plotted S_{11} and S_{41} in the respective Fig. 16 (a) and (c). Meanwhile, degradation also can be noticed for S_{31} and phase difference between output ports presented in Fig. 16 (b) and (d), correspondingly. Whilst, minimal effect due to W_{stub} variation can be observed for S_{21}. Thus, smaller W_{stub} is better compared to larger W_{stub} with the optimal dimension of 0.18 mm. Then with the fixed 0.15 mm W_{slot}, the plotted varied W_{stub} graphs were compared to the summarized measured results in Table 5. Thus, it can be predicted that the fabricated coupler could not have W_{stub} discrepancy from its optimal 0.18 mm. Hence from this analysis, the deviation observed from the measurement results of the proposed coupler compared to the simulation can be due to the fabricated coupler has slightly wider W_{slot} (0.35 mm) than its optimal width of 0.15 mm.

Comparison of the proposed 3-dB BLC with microstrip-slot stub to other designs. Nonetheless, concerning its amplitude deviation, phase deviation, and operating frequency, the proposed design is compared to other coupler designs[37–39] using different techniques. By referring to Table 6, the proposed design has comparable amplitude imbalance, phase imbalance, and bandwidth with the design based on lumped-elements and fabricated using integrated passive devise (IPD) technology on glass substrate proposed by Cayron et al.[37]. Another coupler[38] that fabricated using IPD chip-level technology on gallium arsenide (GaAs) based substrate has higher amplitude imbalance but better phase imbalance compared to the proposed design. While two coupler designs based on the respective substrate integrated waveguide (SIW) and stripline demonstrated higher amplitude imbalance and phase imbalance with narrower bandwidth compared to the proposed design. Hence, by denoting this comparison, the good planar microstrip coupler design with a well-chosen substrate of RT5880

Design	Technique	Amplitude Imbalance	Phase Imbalance	Operating Frequency (GHz)
Proposed Design	Microstrip with microstrip-slot stub impedance	± 1 dB	± 4°	22–30 (BW = 8)
3 dB coupler[37]	Lumped-elements IPD fabrication (Substrate: Glass)	± 0.9 dB	± 3°	19.5–26.5 (BW = 7)
Lange coupler[38]	IPD chip-level fabrication (Substrate: GaAs)	± 1.5 dB	± 2°	26
3 dB coupler[39]	SIW	± 2.7 dB	± 6°	24–28 (BW = 4)
	Stripline	± 1.8 dB	± 6°	24–28 (BW = 4)

Table 6. Comparison of the proposed design with other coupler designs using different techniques. **BW* Bandwidth.

that has a low dielectric constant, very low tan δ, and high Q-factor as shown by this proposed design can offer very well wideband performance even though planar technology faces significant losses at high frequency.

Conclusion

Based on the analysis of dielectric materials that lower loss tangent, tan δ contributes to a higher Q-factor due to dielectric properties, Q_d, while a lower dielectric constant, ε_r results in greater bandwidth performance. Thus, to ensure a device designed at high frequency for 5G application is perform well, the substrate must be selected based on it having a low dielectric constant, ε_r , a low loss tangent, tan δ and a high Q-factor due to dielectric properties, Q_d. Hence, the substrate that displayed the best performance, which was RT5880 due to its lowest ε_r of 2.2, lowest tan δ of 0.0009 and highest Q_d of 1302.79 was selected. Its use in the design was presented with a proposed wideband 3-dB BLC with microstrip-slot stub impedance and overall dimensions of 29.9 mm × 19.9 mm. The design and optimization were conducted using CST Microwave Studio, which is an electromagnetic (EM) simulator. The performances of transmission coefficients, reflection coefficients and phase characteristics of the designed coupler were obtained and analyzed. Its wideband performance at a design frequency of 26 GHz was proven via measurements of the fabricated prototype's performance in the laboratory.

Received: 12 March 2020; Accepted: 27 August 2020
Published online: 30 September 2020

References

1. Asvin, G., Modi, H. & Patel, S. K. 5G technology of mobile communication: a survey. In *IEEE International Conference on Intelligent System and Signal Processing*, 288–292 (2013).
2. Hayashi, H., Hitko, D. A. & Sodini, C. G. Four-element planar Butler matrix using half-wavelength open stubs. *IEEE Microw. Wirel. Compon. Lett.* **12**, 73–75 (2002).
3. Butler, J. & Lowe, R. Beam-forming matrix simplifies design of electronically scanned antennas. *Electron. Des.* **9**, 170–173 (1961).
4. Kalam, S. V. & Rathi, A. B. Optimum design of 4x4 symmetrically structured butler matrix. *Int. J. Sci. Res. Eng. Technol.* **5**, 31–34 (2016).
5. Sahu, B. *Design and Implementation of 4x4 Butler Matrix* (Indian Institute of Science, Bangalore).
6. Bhowmik, W. & Shrivasta, S. Optimum design of 4x4 planar butler matrix array for WLAN application. *J. Telecommun.* **2**, 68–74 (2010).
7. Yang, Q. L., Ban, Y. L., Lian, J. W., Yu, Z. & Wu, B. SIW butler matrix with modified hybrid coupler for slot antenna array. *IEEE Access* **4**, 9561–9569 (2016).
8. Yang, Q. L., Ban, Y. L., Zhou, Q. Q. & Li, M. Y. Butler matrix beamforming network based on substrate integrated technology for 5G mobile devices. In *IEEE Asia-Pacific Conference on Antennas and Propagation (APCAP),* 413–414 (2016).
9. Babale, S. A., Rahim, S. K. A., Barro, O. A. & Khalily, M. Single layered 4 × 4 butler matrix without phase-shifters and crossover. *IEEE Access* **6**, 77289–77298 (2018).
10. Wang, H., Liu, X., Cai, W. & Cao, H. Design and realization of a new compact branch-line coupler using defected ground structure. In *International Conference Solid-State and Integrated-Circuit Technology (ICSICT),* 1376–1379 (2008).
11. Bhowmik, P., Moyra, T. & Deb, P. K. Miniaturization and bandwidth enhancement of a loose coupler by DGS. In *International Conference Signal Processing and Integrated Network (SPIN),* 638–641 (2015).
12. Abdullah, M. A. & Seman, N. The effect of slotline on the bandwidth performance enhancement of branch line coupler. In *Asia-Pacific Conference Applied Electromagnetics (APACE),* 75–78 (2014).
13. Jin, J. & Xu, F. Low-loss, wideband 3db hybrid coupler based on AMC for 5G millimeter-wave application. In *International Symposium on Antennas and Propagation (ISAP)*, 1–4 (2019).
14. Letavin, D.A. and Knyazev, N.S. Study of the influence of dielectric permittivity on effectiveness of branch-line coupler miniaturization. In *IEEE International Conference on Microwaves, Antennas, Communications and Electronic Systems (COMCAS)*, 1–4 (2017).
15. Salleh, M. H. M., Seman, N., Zaidel, D. N. A. & Eteng, A. A. Investigation of unequal planar wireless electricity device for efficient wireless power transfer. *Radioengineering* **26**, 251–257 (2017).
16. Mumin, A. O., Alias, A., Awaleh, A. A. & Abdulhasan, R. A. Assessment of microstrip patch antenna performance based on dielectric substrate. In *International Conference on Computer, Communications, and Control Technology (I4CT)*, 468–471 (2015).
17. Hindle, P., Kimery, J., Aguayo, A., Mattingly, T. & Conrood, J. Selection of PCB Material for 5G. *Microwave Journal e-book*, 1–22 (2018).
18. Nascimento, D. C. & Lacava, J. C. da S. Design of low-cost probe-fed microstrip antennas. In *Microstrip Antennas.* 1–28 (InTech, 2011).
19. Rogers Corporation. Datasheet of RT/duroid® 5870 /5880 High Frequency Laminates (2018).
20. Rogers Corporation. Datasheet of RO4000® Series High Frequency Circuit Materials (2018).
21. Rogers Corporation. Datasheet of TMM® Thermoset Microwave Materials (2018).
22. Rogers Corporation. Datasheet of RT/duroid® 6006/6010LM High Frequency Laminates (2018).
23. Pozar, D. *Microwave Engineering* 3rd edn. (Wiley, New York, 2005).

24. Salleh, M. H. M., Seman, N. & Dewan, R. The investigation of substrate's dielectric properties for improving the performance of witricity devices. *ACES J.* **32**, 24–30 (2017).
25. Khan, A. A., Mandal, M. K. & Sanyal, S. S. Unloaded quality factor of a substrate integrated waveguide resonator and its variation with the substrate parameters. In *International Conference Microwave and Photonics (ICMAP),* 1–4 (2013).
26. Behagi, A. A. & Turner, S. D. *(2015) Microwave and RF Engineering* (BT Mivrowave LLC, State College, 2015).
27. Ohsato, H., Varghese, J. & Jantunen, H. Dielectric losses of microwave ceramics based on crystal structure. In *Electromagnetic Materials*, 1–26 (InTech, 2018).
28. Raveendran, A., Sebastian, M. T. & Raman, S. Applications of microwave materials: a review. *J. Electron. Mater.* **48**, 2601–2634 (2019).
29. Zulkifli, F. Y., Chasanah, N. & Rahardjo, E. T. Design of butler matrix integrated with antenna array for beam forming. In *IEEE International Symposium Antennas and Propagation (ISAP)*, 1–4 (2015).
30. Tutkur, E. Wideband Directional Couplers and Power Splitters. Master Thesis. Chalmers University of Technology Gothenburg, Sweden. (2014).
31. Gomha, S., El-Rabaie, E. S. M. & Shalaby, A. A. T. Optimizing the performance of branch-line couplers using open ended stubs. In *International Conference on Computing, Electrical and Electronic Engineering (ICCEEE),* 363–367 (2013).
32. Ashforth, J. V. Design equations to realise a broadband hybrid ring or a two-branch guide coupler of any coupling coefficient. *Electron. Lett.* **24**, 1276–1277 (1988).
33. Yusof, K. H., Seman, N. & Jamaluddin, M. H. Design of U-shaped in-phase power divider employing ground-slotted technique for wideband applications. *Wirel. Pers. Commun.* **81**, 359–371 (2015).
34. Wu, Q., Yang, Y., Wang, Y., Shi, X. & Yu, M. Characteristic impedance control for branch-line coupler design. *IEEE Microw. Wirel. Compon. Lett.* **28**, 123–125 (2018).
35. Keysight Technology. Keysight Electronic Calibration Module.
36. Maury Microwave, Technical Data 2Z-058C Precision Calibration Solutions (2015).
37. Cayron, A., Viallon, C., Ghannam, A., Magnani, A. & Parra, T. Wideband and compact 3-D quadrature coupler for 5G applications. In *European Microwave Conference (EuMC)* (2019).
38. Liao, Y., Qian, G. & Han, Y. Miniaturized lange bridge design for 5G millimeter waves communication. In *International Applied Computational Electromagnetics Society Symposium—China (ACES)* (2019).
39. Cao, Y-Y., Wu, Y-W., Jiang, Z., & Hao, Z-C. A compact millimeter-wave planar directional coupled crossover with a wide bandwidth. *IEEE Microw. Wirel. Compon. Lett.* **30**, 661–664 (2020).

Acknowledgements

This work was supported by Ministry of Education Malaysia (MOE) and Universiti Teknologi Malaysia (UTM) through Prototype Research Grant Scheme (PRGS) [Vote Number of 4L684]; Fundamental Research Grant Scheme (FRGS) [Vote Number of 5F048]; and HiCoE Grant [Vote Numbers of 4J408].

Author contributions

N.A.M.S. performed the analysis, designed the device, carried out the measurements and wrote the manuscript; N.S. contributed to the overall idea and concept and the preparation of the manuscript through writing, review, editing, and comments. And all authors were involved in modifying the paper, and the literature review.

Competing interests

The authors declare no competing interests.

Additional information

Correspondence and requests for materials should be addressed to N.S.

Reprints and permissions information is available at www.nature.com/reprints.

Publisher's note Springer Nature remains neutral with regard to jurisdictional claims in published maps and institutional affiliations.